Optimizing conditional-π phase shift between two weak coherent pulses via a closed double-Λ atomic system

Gyu-Hyeok Lee,* U-Shin Kim,*,† and Yoon-Ho Kim‡

Department of Physics, Pohang University of Science and Technology (POSTECH), Pohang 37673, South Korea

(Received 10 September 2025; accepted 25 March 2026; published 10 April 2026)

Conditional-π phase shift between two photons is essential for entanglement generation and universal quantum logic. For photons, however, direct conditional controls are not possible and must be mediated by nonlinear media. Achieving such operations for photonic polarization qubits has remained difficult due to intrinsically weak photon-photon nonlinearities in atomic systems. Here, we show that a conditional-π phase shift between two weak coherent pulses can be realized via a cavityless closed double-Λ atomic system, where quantum interference between linear and nonlinear atom-photon interactions enables conditional control. By optimizing the interaction parameters, including amplitude and phase compensations, we identify the conditions for conditional-π phase shift between two weak coherent pulses. Experimentally, we observe the conditional-π phase shift with relative output amplitude 0.74 ± 0.06 and phase shift $(0.95 \pm 0.03)\pi$ between the two-photon amplitudes $|HH\rangle$ and $|VV\rangle$. A theoretical analysis of Bell-state generation from weak coherent pulses further shows Clauser-Horne-Shimony-Holt inequality violation and nonzero concurrence. Our results clarify both the theoretical requirements and the experimental feasibility of cavityless atom-mediated nonlinearities for photonic quantum logic, establishing a scalable route toward nonlinear quantum photonics.

DOI: 10.1103/g75t-x4bj

I. INTRODUCTION

A conditional-π phase shift between two photons is an essential building block for photonic quantum information processing, enabling entanglement generation [1–3] and quantum gate operations such as the controlled-Z (CZ) gate [1,4–7]. However, the experimental implementation of efficient conditional control at the single-photon level remains challenging, since photons do not directly interact in vacuum. Linear- optical approaches can implement the conditional-π phase shift and photonic CZ gate operations by exploiting quantum interference and projective measurements [3,6,7], albeit only probabilistically, since linear optics preserves photon statistics [8–11] and cannot provide deterministic photon-photon interactions. Note also that a complete Bell-state measurement, a key prerequisite for photonic quantum information processing, requires nonlinear photon-photon interactions [12,13]; consequently, linear-optical Bell-state measurements cannot project onto all four Bell states.

In contrast, nonlinear-optical schemes exploit strong photon-photon interactions mediated by atomic media [14], enabling the conditional-π phase shift [15], deterministic gate operations [1,4], and direct manipulation of the quantum nature of light [16–18]. Recent advances in cavity QED and Rydberg-atom platforms have realized enhanced nonlinearities at the single-photon level [4,15,19–22]. Nonetheless, these approaches face inherent scalability limitations, such as stringent stabilization requirements [1,23] and considerable experimental complexity [24,25], motivating the search for simpler and more practical schemes.

A promising direction to implement the efficient conditional control at the single-photon level is to exploit quantum interference between linear and nonlinear atom-photon interactions, which can effectively amplify weak optical nonlinearities [26]. Even with small nonlinear susceptibilities, such interplay enables efficient photon-photon interactions, providing a scalable resource for nonlinear quantum optics [26–31]. Due to its feasibility and versatility, this quantum interference approach has already enabled key demonstrations, including phase-by-phase modulation [29], large cross-phase modulation [30], and nondestructive photon detection [31], thereby offering a practical pathway toward scalable nonlinear quantum optical schemes.

In this work, we demonstrate that a conditional-π phase shift between two weak coherent pulses can be realized in a cavityless closed double-Λ atomic system, where quantum interference between linear and nonlinear atom-photon interactions enables the conditional control. By optimizing the interaction parameters, including amplitude and phase compensations, we identify the conditions for conditional-π phase shift between two weak coherent pulses in the two-photon polarization basis. Experimentally, we observe the conditional-π phase shift with relative output amplitude 0.74 ± 0.06 and phase shift $(0.95 \pm 0.03)\pi$ between two-photon amplitudes

*These authors contributed equally to this work.
†Contact author: usinkimphysics@gmail.com
‡Contact author: yoonho72@gmail.com

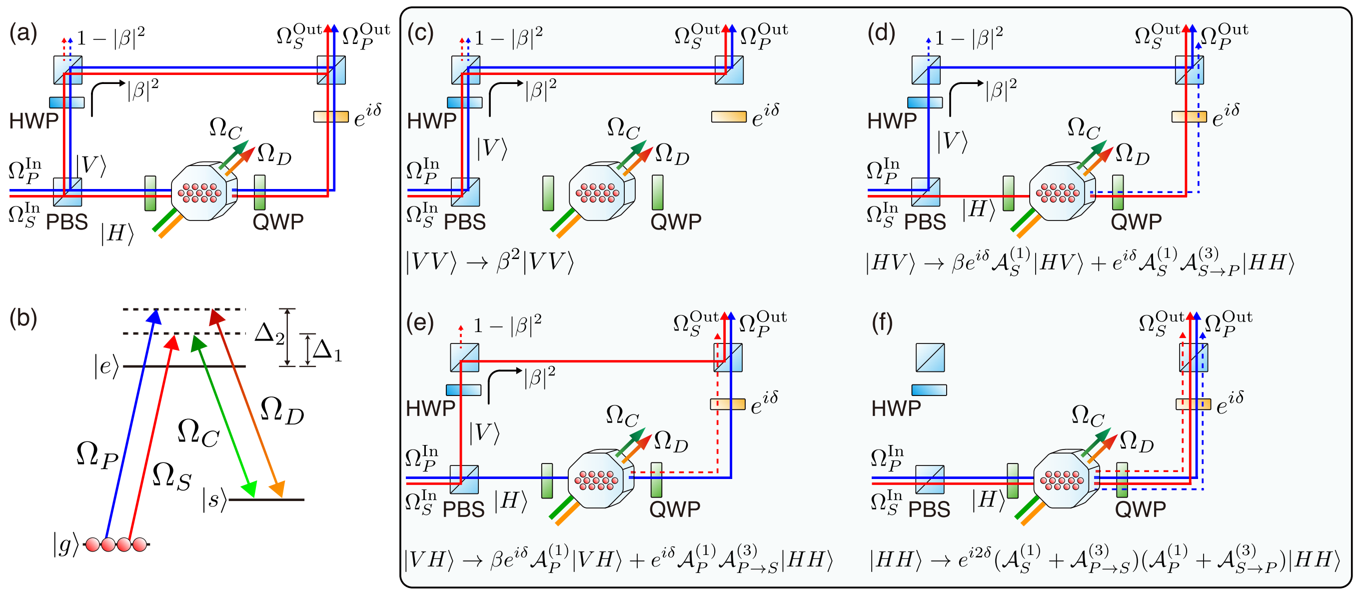

FIG. 1. (a) Schematic for the CZ gate implementation. The input signal (Ω_S^{In}) and probe (Ω_P^{In}) experience both linear and nonlinear atom-light interactions on the lower path of Mach-Zehnder interferometer. The atomic medium is dressed by coupling (Ω_C) and driving (Ω_D) fields, manipulating the atom-light interactions. Also, the amplitude and phase compensations, β and $e^{i\delta}$, respectively, are implemented for CZ gate operation. HWP: (half-wave plate); QWP: (quarter-wave plate); PBS: polarizing beam splitter. (b) The double- Λ-type energy level scheme of ^{87}Rb atoms ($|g\rangle = |5S_{1/2}, F = 1\rangle$, $|s\rangle = |5S_{1/2}, F = 2\rangle$, $|e\rangle = |5P_{1/2}, F' = 2\rangle$). (c)–(f) Schematics of the gate operation for each two-photon polarization input state $\{|VV\rangle, |HV\rangle, |VH\rangle, |HH\rangle\}$. $\mathcal{A}_{S(P)}^{(1)}$ corresponds to the transmission coefficient of signal (probe) pulse, and $\mathcal{A}_{S\rightarrow P(P\rightarrow S)}^{(3)}$ corresponds to the conversion coefficient from signal to probe (probe to signal).

$|HH\rangle$ and $|VV\rangle$. An analysis of Bell-state generation from weak coherent lights further reveals Clauser-Horne-Shimony-Holt (CHSH) inequality violation and nonzero concurrence for the input coherent-state amplitude $|\alpha| < 0.78$, which shows the efficient generation of Bell state from weak coherent lights in our system. Together, these results establish both the theoretical requirements and experimental feasibility of cavityless atom-mediated nonlinearities for weak coherent states, marking a scalable pathway toward nonlinear quantum photonics.

II. THEORETICAL DESCRIPTION

Figure 1(a) shows the schematic of our setup, which integrates the quantum interference between atomic linear and nonlinear responses within a Mach-Zehnder interferometer. Input beams with well-defined polarizations, namely, the signal (Ω_S^{In}) and probe (Ω_P^{In}), are split into two paths by a polarizing beam splitter (PBS). Vertically polarized beams bypass the atomic medium, while horizontally polarized beams interact with the medium dressed by coupling (Ω_C) and driving (Ω_D) fields. When both signal and probe are horizontally polarized, quantum interference between the medium's linear and nonlinear responses induces a conditional-π phase shift between them.

The closed double-Λ system used to induce both linear and nonlinear responses is shown in Fig. 1(b), where we assume the ground-state approximation and balanced coupling and driving fields, i.e., $|\Omega_C| = |\Omega_D|$ [32,33]. The combined effects of the linear and nonlinear responses in our system lead to the transmission ($\Omega_{S(P)}^{\mathrm{In}} \rightarrow \Omega_{S(P)}^{\mathrm{Out}}$) and the frequency conversion ($\Omega_{S(P)}^{\mathrm{In}} \rightarrow \Omega_{P(S)}^{\mathrm{Out}}$) for signal and probe. First, the transmission modulated by the coupling and driving fields results in additional attenuation and phase accumulation [30,34]. Note that the transmission in our system includes both linear and nonlinear responses, where the linear response corresponds to the atomic absorption, and the nonlinear response corresponds to the energy transfer to the other mode due to the stimulated four-wave mixing (FWM) process. The transmission coefficients of the signal and probe under these responses are given as [30,34]

$$\mathcal{A}_S^{(1)} = \mathcal{A}_P^{(1)} = \tfrac{1}{2}(1 + e^{-iD\gamma/(2\tilde{\Delta})}), \tag{1}$$

where $\mathcal{A}_S^{(1)}$ and $\mathcal{A}_P^{(1)}$ are the transmission coefficients for signal and probe, respectively, D is the optical depth (OD) of the atomic medium, γ is the dephasing rate of $|e\rangle$, and $\tilde{\Delta} = (\Delta_1 + \Delta_2) + i\gamma$, where Δ_1 and Δ_2 are the one-photon detunings of signal and probe, respectively.

In contrast, the frequency conversion purely arises from the nonlinear response via the stimulated FWM process, where the signal can be converted into the probe, and vice versa. Then, the conversion coefficients of the signal and probe under the nonlinear response are given by [30,34]

$$\begin{aligned} \mathcal{A}_{S\rightarrow P}^{(3)} &= \tfrac{1}{2}(1 - e^{-iD\gamma/(2\tilde{\Delta})})e^{-i\phi_r}, \\ \mathcal{A}_{P\rightarrow S}^{(3)} &= \tfrac{1}{2}(1 - e^{-iD\gamma/(2\tilde{\Delta})})e^{i\phi_r}, \end{aligned} \tag{2}$$

where $\mathcal{A}_{S\rightarrow P}^{(3)}$ denotes the conversion coefficient from signal to probe, and $\mathcal{A}_{P\rightarrow S}^{(3)}$ from probe to signal. Here, $\phi_r = \phi_C - \phi_D$, with ϕ_C and ϕ_D the phases of the coupling and driving fields, respectively.

To achieve a conditional-π phase shift between two-photon amplitudes $|HH\rangle$ and $|VV\rangle$, compensations in both amplitude and phase are required. As shown in Fig. 1(a), we consider an amplitude compensation in $|V\rangle$ path with a transmission β and a phase compensation in $|H\rangle$ path with an extra phase of $e^{i\delta}$. Then, for a weak coherent light input truncated to the one-photon subspace under the linear and nonlinear atom-photon interactions described in Eqs. (1) and (2), the total operation of our system shown in Figs. 1(c)–1(f) in the polarization basis is given by [35]

$$\begin{aligned}
&|HH\rangle \rightarrow e^{i2\delta}\big(\mathcal{A}_S^{(1)} + \mathcal{A}_{P\to S}^{(3)}\big)\big(\mathcal{A}_P^{(1)} + \mathcal{A}_{S\to P}^{(3)}\big)|HH\rangle,\\
&|HV\rangle \rightarrow \beta e^{i\delta}\mathcal{A}_S^{(1)}|HV\rangle + e^{i\delta}\mathcal{A}_S^{(1)}\mathcal{A}_{S\to P}^{(3)}|HH\rangle,\\
&|VH\rangle \rightarrow \beta e^{i\delta}\mathcal{A}_P^{(1)}|VH\rangle + e^{i\delta}\mathcal{A}_P^{(1)}\mathcal{A}_{P\to S}^{(3)}|HH\rangle,\\
&|VV\rangle \rightarrow \beta^2|VV\rangle.
\end{aligned} \tag{3}$$

The experimental parameters are optimized so that the diagonal elements reproduce the CZ gate, i.e., $[-1, 1, 1, 1]$. First, the complex amplitudes of the $|VV\rangle$, $|VH\rangle$, and $|HV\rangle$ outputs must be equal, which requires

$$\mathcal{A}_S^{(1)} = \mathcal{A}_P^{(1)} = \beta e^{-i\delta}, \tag{4}$$

yielding $\beta = |\mathcal{A}_{S,P}^{(1)}|$ and $\delta = -\arg[\mathcal{A}_{S,P}^{(1)}]$.

Second, the $|HH\rangle$ output must acquire a π-phase shift relative to the $|VV\rangle$ output, expressed as

$$e^{i2\delta}\big(\mathcal{A}_S^{(1)} + \mathcal{A}_{P\to S}^{(3)}\big)\big(\mathcal{A}_P^{(1)} + \mathcal{A}_{S\to P}^{(3)}\big) = -\beta^2. \tag{5}$$

Equations (4) and (5) can be combined into a single parameter that characterizes the conditional-π phase shift:

$$\mathcal{A}_\pi = \frac{\big(\mathcal{A}_S^{(1)} + \mathcal{A}_{P\to S}^{(3)}\big)\big(\mathcal{A}_P^{(1)} + \mathcal{A}_{S\to P}^{(3)}\big)}{\mathcal{A}_S^{(1)}\mathcal{A}_P^{(1)}} = -1, \tag{6}$$

where the amplitude and phase of $\mathcal{A}_\pi$ correspond to the output amplitude ratio and phase shift between $|HH\rangle$ and $|VV\rangle$, respectively. Thus, a conditional-π phase shift requires $|\mathcal{A}_\pi| = 1$ and $\arg[\mathcal{A}_\pi] = \pi$. The amplitude ($\beta$) and phase ($e^{i\delta}$) compensations are not implemented in the experiment and considered only in postprocessing, since the conditional-π phase shift can be directly verified by measuring $\mathcal{A}_\pi = -1$, which is independent of both β and δ.

$$\beta^2\begin{pmatrix} -1 & \mathcal{A}_{S\to P}^{(3)}/\beta & \mathcal{A}_{P\to S}^{(3)}/\beta & 0\\ 0 & 1 & 0 & 0\\ 0 & 0 & 1 & 0\\ 0 & 0 & 0 & 1 \end{pmatrix}. \tag{7}$$

Equation (7) presents the gate operation in two-photon polarization basis $\{|HH\rangle, |HV\rangle, |VH\rangle, |VV\rangle\}$ under optimized parameters satisfying Eqs. (4)–(6). Under these conditions, the diagonal elements exhibit equal output amplitudes with a conditional-π phase shift for $|HH\rangle$. In experiment, the target experimental conditions $D = 53.1$, $\Delta_1 = 0$, $\Delta_2 = 80$ MHz, $\beta = 0.541$, $\delta = 0.859$ rad, and $\phi_r = 101.92^\circ$ satisfy Eqs. (4)–(6), and thus optimize the conditional-π phase shift. While this optimization enables the conditional-π phase shift, two limitations prevent ideal CZ gate operation. First, residual atomic absorption reduces the diagonal amplitudes below unity, leading to the average gate success probability of $\tilde{P}_{\text{succ}} = 17.16\%$ under the target experimental conditions [35]. Second, nonzero transition amplitudes for $|HV\rangle \rightarrow |HH\rangle$ and $|VH\rangle \rightarrow |HH\rangle$ generate additional noise, which must vanish for an ideal CZ gate. Under the target experimental conditions, the off-diagonal noises limit the conditional average gate fidelity as $\mathcal{F}_{\text{con}} = 0.60$ [35]. Note that the noise terms arise from the input coherent state, and when single-photons are considered as the input states, the gate operation becomes the ideal CZ gate as the noise terms vanish [35].

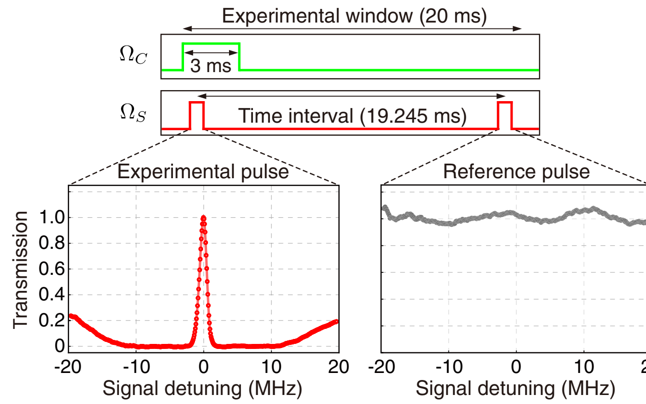

FIG. 2. The experimental sequence to measure the amplitude and phase shift of the output beams. The experimental pulse measures the linear and nonlinear atomic responses, while the reference pulse bypasses the interactions due to the atomic diffusion.

III. EXPERIMENT

We now describe the experimental setup. All four optical fields in the double-Λ level scheme are coherently prepared using two external-cavity diode lasers (ECDLs) that are phase locked via an optical injection-locking method. The 795-nm master laser is locked at -120 MHz from the $|5S_{1/2}, F = 2\rangle \leftrightarrow |5P_{1/2}, F' = 2\rangle$ transition. The coupling (Ω_C) and driving (Ω_D) fields are prepared from the master laser and set to be on resonance and 80 MHz blue detuned, respectively, by modulating the frequencies by $+120$ and $+200$ MHz using acousto-optic modulators (AOMs). A separate branch of the master laser is upshifted by 6.79 GHz using an electro-optic modulator to seed the second ECDL and achieve the optical injection locking. The 795-nm seeded laser is then locked at -160 MHz from the $|5S_{1/2}, F = 1\rangle \leftrightarrow |5P_{1/2}, F' = 2\rangle$ transition. The signal (Ω_S) and probe (Ω_P) are prepared from the seeded laser and set to be on resonance and 80 MHz blue detuned, respectively, by modulating the frequencies by $+160$ and $+240$ MHz using AOMs. As the optical powers of the signal and probe do not affect the transmission and conversion coefficients under the balanced condition ($\Omega_C = \Omega_D$), their powers are adjusted to approximately 300–500 μW to optimize the output measurements.

A cigar-shaped ^{87}Rb atomic ensemble is prepared in a magneto-optical trap. Each experimental sequence lasts 200 ms, with 180 ms devoted to preparing the cold atomic medium, yielding a maximum optical depth of about 100. In the remaining 20-ms window (Fig. 2), two signal (probe) pulses, prepared as weak coherent states, are sent through the medium, separated by 19.345 ms. The early pulse (experimental) experiences the linear and nonlinear atom-photon interactions of the double-Λ system, while the late pulse

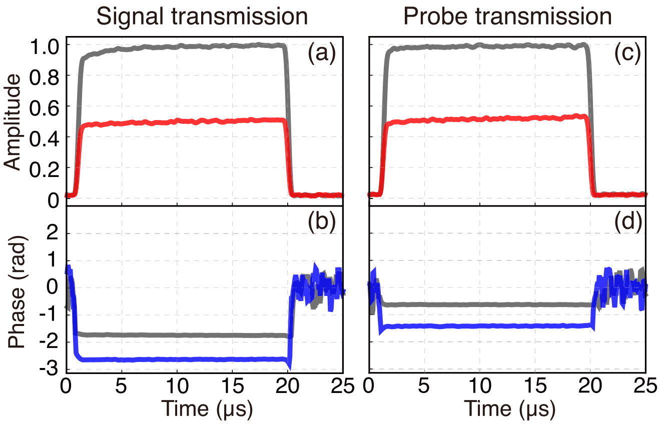

FIG. 3. (a), (b) The amplitude (red line) and phase (blue line) of signal transmission coefficient $\mathcal{A}_S^{(1)}$, respectively. (c), (d) The amplitude (red line) and phase (blue line) of probe transmission coefficient $\mathcal{A}_P^{(1)}$, respectively. Gray lines are the measurement outcomes from the reference pulses for each amplitude and phase measurements.

(reference) bypasses such interactions, as the atoms have diffused away during the long interval. The atomic diffusion is verified by comparing the atomic absorption of the experimental and reference pulses, as shown in Fig. 2. The experimental pulse exhibits an atomic absorption with a narrow electromagnetically induced transparency window, whereas no atomic absorption is observed for the reference pulse, which bypasses any atom-photon interactions. Therefore, the transmission and conversion coefficients of the signal and probe are obtained by comparing the complex amplitudes of the experimental and reference pulses.

The complex amplitudes of the transmission and conversion coefficients are measured using beat-note interferometry [35,39–41], which provides both normalized amplitude and phase shift induced by the atomic response. In this method, a 795-nm local oscillator (LO) beam is overlapped with the signal and probe before the atomic medium. The LO does not interact with the medium owing to its large red detuning from $|5S_{1/2}, F = 1\rangle \leftrightarrow |5P_{1/2}, F' = 2\rangle$ transition ($\Delta_{\mathrm{LO}} = -280$ MHz). The frequency offsets between the LO and the signal (probe) beams are set to 280 (360) MHz, producing two beat notes at 280 and 360 MHz that are separately detected on a high-bandwidth photodetector. In addition, the interference between the signal and probe yields a third beat note at 80 MHz, corresponding to $\Delta_2 - \Delta_1$. The beat notes are processed via in-phase/quadrature (I/Q) demodulation to extract both amplitude and phase simultaneously, yielding the transmission and conversion coefficients of the signal and probe.

IV. RESULTS

Figure 3 shows the normalized amplitude and phase shift measurements for the signal and probe. A 20 μs signal (probe) pulse is injected into the atomic medium in the absence of the probe (signal) pulse, so that the transmission coefficients ($\mathcal{A}_S^{(1)}$ and $\mathcal{A}_P^{(1)}$) can be directly measured. Figures 3(a) and 3(b) display the amplitude and phase of the signal transmission coefficient $\mathcal{A}_S^{(1)}$, while Figs. 3(c) and 3(d) show those of the probe transmission coefficient $\mathcal{A}_P^{(1)}$.

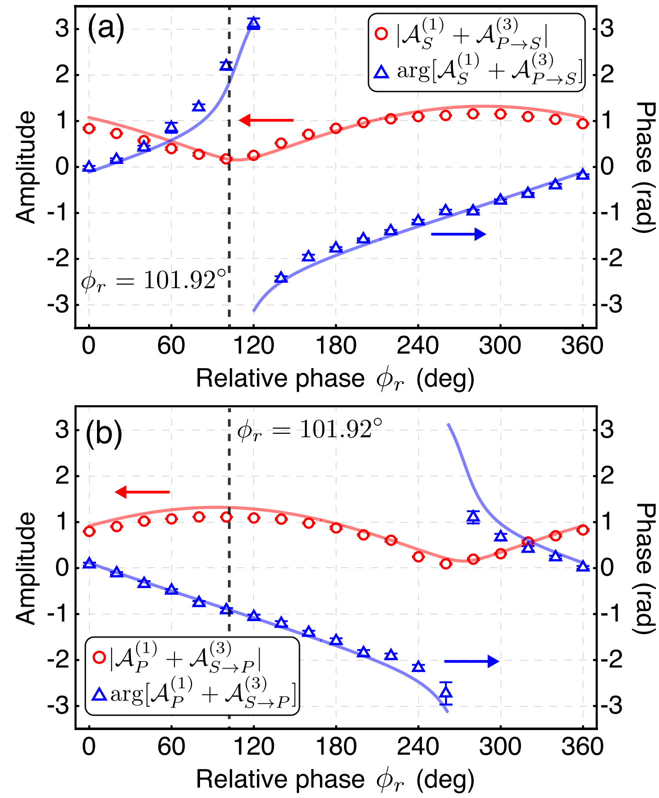

FIG. 4. (a) The normalized amplitude (red circle) and phase shift (blue triangle) of signal output ($\mathcal{A}_S^{(1)} + \mathcal{A}_{P\to S}^{(3)}$) with respect to the relative phase ϕ_r. (b) The normalized amplitude (red circle) and phase shift (blue triangle) of probe output ($\mathcal{A}_P^{(1)} + \mathcal{A}_{S\to P}^{(3)}$) with respect to the relative phase ϕ_r. Solid lines are the theoretical curves with fitting parameters of $D = 50.0$, $\Delta_1 = 0$, and $\Delta_2 = 80$ MHz. Error bars are displayed on the experimental data, but some are too small to be visualized.

The output amplitudes are reduced relative to the reference pulse, consistent with conversion of signal (probe) into probe (signal) via the stimulated FWM process. The negative phase shifts observed in both cases are explained by the phase accumulation in Eq. (1). From the amplitude and phase data, the transmission coefficients $\mathcal{A}_{S,P}^{(1)}$ are obtained. Averaging over 20 datasets in the 3–17 μs window yields $\mathcal{A}_S^{(1)} = (0.506 \pm 0.008)\exp[i(-0.897 \pm 0.012)]$ and $\mathcal{A}_P^{(1)} = (0.521 \pm 0.012)\exp[i(-0.789 \pm 0.018)]$.

Figure 4 shows the amplitude and phase measurements as a function of the relative phase ϕ_r between the coupling and driving fields, with both signal and probe injected into the atomic medium. In this case, all optical fields in the double-Λ system interact, and beat-note interferometry measures the combined linear and nonlinear responses: the output signal corresponds to ($\mathcal{A}_S^{(1)} + \mathcal{A}_{P\to S}^{(3)}$) [Fig. 4(a)], and the output probe to ($\mathcal{A}_P^{(1)} + \mathcal{A}_{S\to P}^{(3)}$) [Fig. 4(b)]. The observed ϕ_r dependence reflects interference between linear and nonlinear atomic responses, as described by Eqs. (1) and (2). The relative phase ϕ_r is controlled by varying the RF phase of the AOM applied to the driving field (Ω_D). The solid lines represent theoretical curves from Eqs. (1) and (2) with fitting parameters $D = 50.0$, $\Delta_1 = 0$, and $\Delta_2 = 80$ MHz, showing good agreement with the data. The

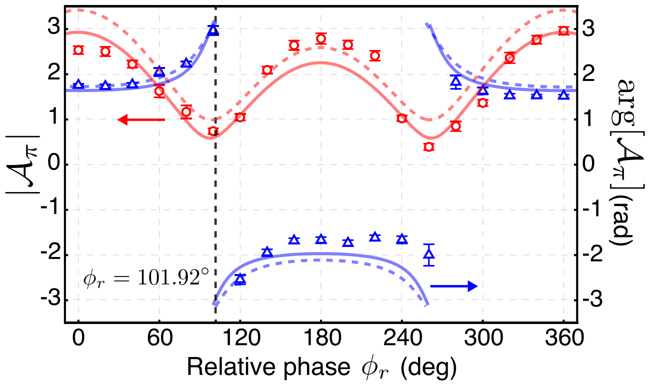

FIG. 5. The normalized amplitude (red circle) and phase shift (blue triangle) of $\mathcal{A}_\pi$. The solid lines are the theoretical curves with fitting parameters of $D = 50.0$, $\Delta_1 = 0$, and $\Delta_2 = 80\,\text{MHz}$. The dashed lines are the theoretical curves under $D = 53.1$ with the same detunings, which achieve $\mathcal{A}_\pi = -1$.

phase error bars increase at the amplitude minima because weaker beat-note signals yield noisier phase measurements. From these results, we estimate the conversion coefficients as $\mathcal{A}^{(3)}_{S\to P} e^{i\phi_r} = (0.609 \pm 0.022)\exp[i(0.795 \pm 0.041)]$ and $\mathcal{A}^{(3)}_{P\to S} e^{-i\phi_r} = (0.649 \pm 0.027)\exp[i(0.639 \pm 0.048)]$.

Figure 5 shows the amplitude and phase of $\mathcal{A}_\pi$ as a function of the relative phase ϕ_r, corresponding to the relative amplitude and phase of the $|HH\rangle$ output with respect to the $|VV\rangle$ output. $\mathcal{A}_\pi$ is obtained from the transmission and conversion coefficients measured in Figs. 3 and 4. Experimentally, we measure the maximum phase shift of $\arg[\mathcal{A}_\pi] = (0.95 \pm 0.03)\pi$ with $|\mathcal{A}_\pi| = 0.74 \pm 0.06$, whereas the target CZ condition requires $\mathcal{A}_\pi = -1$ [Eq. (7)]. The discrepancy in $|\mathcal{A}_\pi|$ arises primarily from optical depth fluctuations in the experiment. The solid line in Fig. 5 represents the theoretical curve with fitting parameters $D = 50.0$, $\Delta_1 = 0$, and $\Delta_2 = 80$ MHz, showing good agreement with the data. The dashed line shows the theoretical prediction under the target condition ($D = 53.1$, same detunings), for which $\mathcal{A}_\pi = -1$ is achieved at $\phi_r = 101.92°$. This comparison indicates that the main limitation in $|\mathcal{A}_\pi|$ originates from OD fluctuations. We expect that this imperfection can be mitigated by fine-tuning either the OD or the one-photon detuning Δ_2.

Finally, we theoretically analyze the quality of Bell states generated by a controlled-not (CNOT) gate, which can be implemented by a CZ gate followed by a local Hadamard operation ($\hat{I} \otimes \hat{H}$). Note that the local Hadamard operation can be achieved by a half-wave plate with a fast axis angle of $\pi/8$. We consider the CZ gate under the target condition, including amplitude and phase compensations (β and δ) under the corresponding target conditions satisfying Eqs. (4)–(6) as $D = 53.1$, $\Delta_1 = 0$, $\Delta_2 = 80\,\text{MHz}$, and $\phi_r = 101.92°$ ($\beta = 0.549$ and $\delta = 0.859$). The corresponding gate operation given in Eq. (7) leads to

$$0.293 \times \begin{pmatrix} -1 & 0.493 - 1.325i & 0.987 + 1.012i & 0 \\ 0 & 1 & 0 & 0 \\ 0 & 0 & 1 & 0 \\ 0 & 0 & 0 & 1 \end{pmatrix}. \tag{8}$$

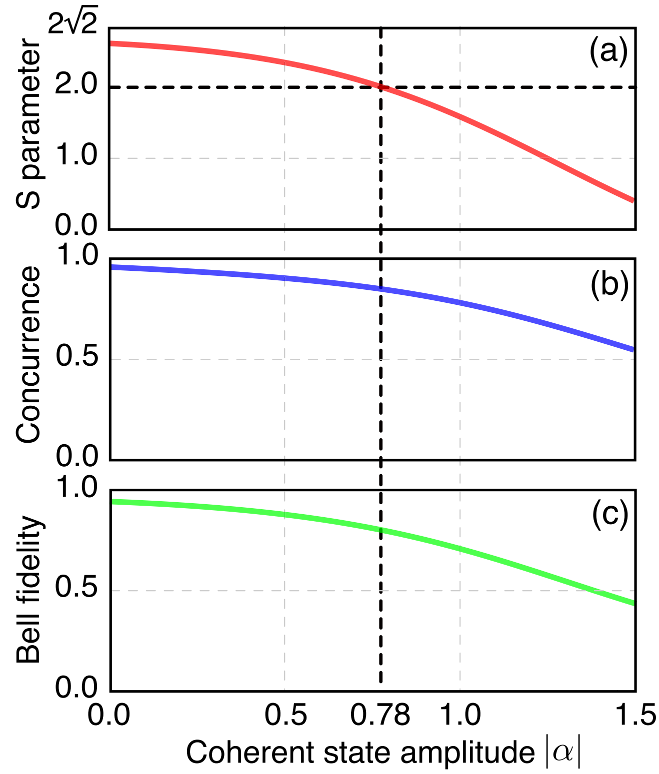

FIG. 6. (a) The CHSH S parameter, (b) the concurrence, and (c) the Bell-state fidelity of the output two-photon state after the controlled-not gate operation. The CZ gate is considered as Eq. (7). The maximal photon number of coherent state is truncated to ten-photon subspace.

The input quantum state is taken as $|\alpha\rangle^S_A|\alpha\rangle^P_A$, where $|\alpha\rangle$ is a coherent state with mean photon number $|\alpha|^2$, the subscript A denotes the antidiagonal polarization state ($-45°$), and the superscript S (P) refers to the signal (probe). For analysis, the coherent state is truncated to the ten-photon subspace, i.e., $|\alpha\rangle \approx \mathcal{N}\sum_{n=0}^{10}(\alpha^n/\sqrt{n!})|n\rangle$, where $\mathcal{N}$ denotes the normalization factor. Coincidence detection with threshold single-photon detectors filters out the vacuum component and traces out the Fock basis, yielding a partially entangled Bell state in the polarization basis. Figures 6(a) and 6(b) show the CHSH S parameter and the concurrence of the output two-photon state, respectively [35]. The CHSH S parameter is estimated as $S = \langle\hat{A}_0\hat{B}_0\rangle + \langle\hat{A}_0\hat{B}_1\rangle + \langle\hat{A}_1\hat{B}_0\rangle - \langle\hat{A}_1\hat{B}_1\rangle$ for $\hat{A}_0 = \hat{\sigma}_x$, $\hat{B}_0 = \hat{\sigma}_z$, $\hat{A}_1 = (\hat{\sigma}_x + \hat{\sigma}_z)/\sqrt{2}$, and $\hat{B}_1 = (\hat{\sigma}_x - \hat{\sigma}_z)/\sqrt{2}$. For $|\alpha| < 0.78$, the S parameter exceeds 2, demonstrating CHSH inequality violation and thus nonlocal correlations [42]. Moreover, the non-zero concurrence values across the $|\alpha|$ range confirm that the output two-photon state possesses nonzero entanglement, where the concurrence C exhibits $C \gtrsim 0.85$ for $|\alpha| < 0.78$. It indicates that our system can effectively generate entangled photon pairs even though the CZ gate operation is not ideal. Figure 6(c) shows the corresponding Bell-state fidelity of the output two-photon state for the coherent-state amplitude $|\alpha|$. For the coherent amplitude exhibiting the nonlocal correlations, $|\alpha| < 0.78$, the Bell-state fidelity of the output state achieves $\mathcal{F}_{\text{Bell}} \gtrsim 0.8$, which reveals the generation of Bell states from weak coherent light input.

Note that the S parameter, concurrence, and the Bell-state fidelity cannot reach their maximum, even for arbitrarily small $|\alpha|$, because the noise arising from $|HV\rangle, |VH\rangle \rightarrow |HH\rangle$ transitions results in a nonmaximally entangled output quantum state.

We further theoretically analyze the optimization of CZ gate operation for single-photon input ($|1\rangle^S|1\rangle^P$) in the Supplemental Material, where the off-diagonal noise vanishes but an atomic medium with a much higher optical depth ($D > 200$) is required compared to the case of coherent light input ($D = 53.1$) [35]. The difference arises from interference between linear and nonlinear atomic responses (i.e., ϕ_r-dependent atomic responses), which gives coincidence detection outcomes only for coherent light input. For single-photon inputs, the interference generates photon-number-bunched components in the output state ($|2\rangle^S|0\rangle^P$ or $|0\rangle^S|2\rangle^P$). While these terms do not contribute to coincidence detection outcomes, they induce leakage from the logical qubit subspace, preventing the direct concatenation of gates without heralding or feedforward operations [8,43,44]. This highlights a unique feature of our system: a classical state input provides a more feasible approach to generating entanglement than a quantum state input.

To overcome both the unavoidable off-diagonal noise arising from coherent-state inputs [27,28,30] and the impractical optical depth requirement associated with single-photon inputs, we propose an optimized CZ gate based on sequential atom-light interactions in our system using single-photon inputs (see Supplemental Material for details) [35]. In this case, the photon-number-bunched components generated from single-photon inputs after the first interaction ($|2\rangle^S|0\rangle^P$ or $|0\rangle^S|2\rangle^P$) contribute to the coincidence detection outcomes after the second interaction, through the interference between the linear and nonlinear interactions (i.e., the ϕ_r-dependent atomic responses). As a result, the CZ gate operation can be optimized without the off-diagonal noises under the experimentally feasible optical depth requirements ($D_1 = 30$ and $D_2 = 25.45$). This shows that an ideal CZ gate operation (with a limited success probability) can be achieved under practical experimental conditions in our system.

V. CONCLUSION

In conclusion, we have demonstrated the optimized conditional-π phase shift in a cavityless closed double-Λ atomic system by exploiting quantum interference between linear and nonlinear atom-photon interactions. We theoretically identified the conditions for the conditional-π phase shift between two weak coherent pulses, including amplitude and phase compensations, and experimentally observed the essential feature of a conditional-π phase shift with relative output amplitude (0.74 ± 0.06) and phase shift $(0.95 \pm 0.03)\pi$ for $|HH\rangle$ relative to $|VV\rangle$. Furthermore, the theoretical analysis on Bell-state generation revealed CHSH inequality violation and nonzero concurrence for weak coherent-state inputs with $|\alpha| < 0.78$. These results establish both the theoretical requirements and experimental feasibility of cavityless atom-mediated nonlinearities for photonic quantum logic, marking a scalable pathway toward nonlinear quantum photonics.

ACKNOWLEDGMENTS

This work was supported by the Samsung Science and Technology Foundation under Grant No. SSTFBA2202-05, by the National Research Foundation of Korea (Grants No. RS-2023-00208500 and No. RS-2024-00442762), and by the Institute of Information & Communications Technology Planning & Evaluation (IITP) grant funded by the Korea government (MSIT) (Grant No. RS-2025-02263264), and Institute of Information & Communications Technology Planning & Evaluation (IITP) ITRC support program (Grant No. IITP-2025-RS-2022-00164799).

DATA AVAILABILITY

The data that support the findings of this article are openly available [45].

[1] A. Reiserer, N. Kalb, G. Rempe, and S. Ritter, A quantum gate between a flying optical photon and a single trapped atom, Nature (London) **508**, 237 (2014).
[2] X. L. Zhang, L. Isenhower, A. T. Gill, T. G. Walker, and M. Saffman, Deterministic entanglement to two neutral atoms via Rydberg blockade, Phys. Rev. A **82**, 030306(R) (2010).
[3] N. K. Langford, T. J. Weinhold, R. Prevedel, K. J. Resch, A. Gilchrist, J. L. O'Brien, G. J. Pryde, and A. G. White, Demonstration of a simple entangling optical gate and its use in Bell-state analysis, Phys. Rev. Lett. **95**, 210504 (2005).
[4] B. Hacker, S. Welte, G. Rempe, and S. Ritter, A photon-photon quantum gate based on a single atom in an optical resonator, Nature (London) **536**, 193 (2016).
[5] L. Isenhower, E. Urban, X. L. Zhang, A. T. Gill, T. Henage, T. A. Johnson, T. G. Walker, and M. Saffman, Demonstration of a neutral atom controlled-NOT quantum gate, Phys. Rev. Lett. **104**, 010503 (2010).
[6] N. Kiesel, C. Schmid, U. Weber, R. Ursin, and H. Weinfurter, Linear optics controlled-phase gate made simple, Phys. Rev. Lett. **95**, 210505 (2005).
[7] R. Okamoto, H. F. Hofmann, S. Takeuchi, and K. Sasaki, Demonstration of an optical quantum controlled-not gate without path interference, Phys. Rev. Lett. **95**, 210506 (2005).
[8] J. Eisert, Optimizing linear optics quantum gates, Phys. Rev. Lett. **95**, 040502 (2005).
[9] D. B. Uskov, L. Kaplan, A. M. Smith, S. D. Huver, and J. P. Dowling, Maximal success probabilities of linear-optical quantum gates, Phys. Rev. A **79**, 042326 (2009).
[10] E. Knill, Bounds on the probability of success of postselected nonlinear sign shifts implemented with linear optics, Phys. Rev. A **68**, 064303 (2003).
[11] E. Knill, Quantum gates using linear optics and postselection, Phys. Rev. A **66**, 052306 (2002).
[12] N. Lütkenhaus, J. Calsamiglia, and K.-A. Suominen, Bell measurements for teleportation, Phys. Rev. A **59**, 3295 (1999).

[13] Y.-H. Kim, S. P. Kulik, and Y. Shih, Quantum teleportation of a polarization state with a complete Bell state measurement, Phys. Rev. Lett. **86**, 1370 (2001).

[14] D. E. Chang, V. Vuletić, and M. D. Lukin, Quantum nonlinear optics—photon by photon, Nat. Photon. **8**, 685 (2014).

[15] D. Tiarks, S. Schmidt, G. Rempe, and S. Dürr, Optical π phase shift created with a single-photon pulse, Sci. Adv. **2**, e1600036 (2016).

[16] S. H. Cantu, A. V. Venkatramani, W. Xu, L. Zhou, B. Jelenković, M. D. Lukin, and V. Vuletić, Repulsive photons in a quantum nonlinear medium, Nat. Phys. **16**, 921 (2020).

[17] O. Firstenberg, T. Peyronel, Q.-Y. Liang, A. V. Gorshkov, M. D. Lukin, and V. Vuletić, Attractive photons in a quantum nonlinear medium, Nature (London) **502**, 71 (2013).

[18] T. Peyronel, O. Firstenberg, Q.-Y. Liang, S. Hofferberth, A. V. Gorshkov, T. Pohl, M. D. Lukin, and V. Vuletić, Quantum nonlinear optics with single photons enabled by strongly interacting atoms, Nature (London) **488**, 57 (2012).

[19] K. M. Beck, M. Hosseini, Y. Duan, and V. Vuletić, Large conditional single-photon cross-phase modulation, Proc. Natl. Acad. Sci. USA **113**, 9740 (2016).

[20] W. Chen, K. M. Beck, R. Bücker, M. Gullans, M. D. Lukin, H. Tanji-Suzuki, and V. Vuletić, All-optical switch and transistor gated by one stored photon, Science **341**, 768 (2013).

[21] D. Tiarks, S. Schmidt-Eberle, T. Stolz, G. Rempe, and S. Dürr, A photon-photon quantum gate based on Rydberg interactions, Nat. Phys. **15**, 124 (2019).

[22] T. Stolz, H. Hegels, M. Winter, B. Röhr, Y.-F. Hsiao, L. Husel, G. Rempe, and S. Dürr, Quantum-logic gate between two optical photons with an average efficiency above 40%, Phys. Rev. X **12**, 021035 (2022).

[23] A. Reiserer, S. Ritter, and G. Rempe, Nondestructive detection of an optical photon, Science **342**, 1349 (2013).

[24] E. Oh, X. Lai, J. Wen, and S. Du, Distributed quantum computing with photons and atomic memories, Adv. Quantum Technol. **6**, 2300007 (2023).

[25] O. Firstenberg, C.-S. Adams, and S. Hofferberth, Nonlinear quantum optics mediated by Rydberg interactions, J. Phys. B: At. Mol. Opt. Phys. **49**, 152003 (2016).

[26] N. K. Langford, S. Ramelow, R. Prevedel, W. J. Munro, G. J. Milburn, and A. Zeilinger, Efficient quantum computing using coherent photon conversion, Nature (London) **478**, 360 (2011).

[27] C.-K. Chiu, Y.-H. Chen, Y.-C. Chen, I. A. Yu, Y.-C. Chen, and Y.-F. Chen, Low-light-level four-wave mixing by quantum interference, Phys. Rev. A **89**, 023839 (2014).

[28] S. Sagona-Stophel, R. Shahrokhshahi, B. Jordaan, M. Namazi, and E. Figueroa, Conditional π-Phase shift of single-photon-level pulses at room temperature, Phys. Rev. Lett. **125**, 243601 (2020).

[29] M. Artoni and A. Zavatta, Large phase-by-phase modulations in atomic interfaces, Phys. Rev. Lett. **115**, 113005 (2015).

[30] Z.-Y. Liu, Y.-H. Chen, Y.-C. Chen, H.-Y. Lo, P.-J. Tsai, I. A. Yu, Y.-C. Chen, and Y.-F. Chen, Large cross-phase modulations at the few-photon level, Phys. Rev. Lett. **117**, 203601 (2016).

[31] K. Xia, M. Johnsson, P. L. Knight, and J. Twamley, Cavity-free scheme for nondestructive detection of a single optical photon, Phys. Rev. Lett. **116**, 023601 (2016).

[32] L. Deng and M. G. Payne, Achieving induced transparency with one- and three-photon destructive interference in a two-mode, three-level, double-Λ system, Phys. Rev. A **71**, 011803(R) (2005).

[33] H. Kang, G. Hernandez, J. Zhang, and Y. Zhu, Phase-controlled light switching at low light levels, Phys. Rev. A **73**, 011802(R) (2006).

[34] Z.-Y. Liu, J.-T. Xiao, J.-K. Lin, J.-J. Wu, J.-Y. Juo, C.-Y. Cheng, and Y.-F. Chen, High-efficiency backward four-wave mixing by quantum interference, Sci. Rep. **7**, 15796 (2017).

[35] See Supplemental Material at http://link.aps.org/supplemental/10.1103/g75t-x4bj for detailed theoretical analysis, which includes Refs. [36–38].

[36] D. McGloin, M. H. Dunn, and D. J. Fulton, Polarization effects in electromagnetically induced transparency, Phys. Rev. A **62**, 053802 (2000).

[37] B. Wang, S. Li, J. Ma, H. Wang, K. C. Peng, and M. Xiao, Controlling the polarization rotation of an optical field via symmetry in electromagnetically induced transparency, Phys. Rev. A **73**, 051801(R) (2006).

[38] M. Horodecki, P. Horodecki, and R. Horodecki, General teleportation channel, singlet fraction, and quasidistillation, Phys. Rev. A **60**, 1888 (1999).

[39] H.-Y. Lo, P.-C. Su, Y.-W. Cheng, P.-I. Wu, and Y.-F. Chen, Femtowatt-light-level phase measurement of slow light pulses via beat-note interferometer, Opt. Express **18**, 18498 (2010).

[40] A. Feizpour, M. Hallaji, G. Dmochowski, and A. M. Steinberg, Observation of the nonlinear phase shift due to single post-selected photons, Nat. Phys. **11**, 905 (2015).

[41] K.-K. Park, J.-H. Kim, T.-M. Zhao, Y.-W. Cho, and Y.-H. Kim, Measuring the frequency-time two-photon wavefunction of narrowband entangled photons from cold atoms via stimulated emission, Optica **4**, 1293 (2017).

[42] J. F. Clauser, M. A. Horne, A. Shimony, and R. A. Holt, Proposed experiment to test local hidden-variable theories, Phys. Rev. Lett. **23**, 880 (1969).

[43] T. C. Ralph, N. K. Langford, T. B. Bell, and A. G. White, Linear optical controlled-NOT gate in the coincidence basis, Phys. Rev. A **65**, 062324 (2002).

[44] P. Kok, W. J. Munro, K. Nemoto, T. C. Ralph, J. P. Dowling, and G. J. Milburn, Linear optical quantum computing with photonic qubits, Rev. Mod. Phys. **79**, 135 (2007).

[45] G.-H. Lee, U-S. Kim, and Y.-H. Kim, Data Set: Optimizing controlled-Z gate for photonic polarization qubits via a closed double- atomic system, available at: https://qoqi.postech.ac.kr/qoqi/bbs/data-set.do?mode=view&articleNo=35161&article.offset=0&articleLimit=10.